Composition of CNT and WO_3 nanoplate: Synthesis and NH_3 gas sensing characteristics at low temperature

Xuan Vuong LE[1], Vu Truong DUONG[1,2], Lan Anh Luu THI[1], Van Thang PHAM[1], Huu Lam NGUYEN[1,3,*], and Cong Tu NGUYEN[1,*]

[1] *School of Engineering Physics, Hanoi University of Science and Technology, No. 1 Dai Co Viet Street, Hanoi 100000, Viet Nam*
[2] *Hanoi Univertisty of Industry, No. 298 Cau Dien Street,100000 Hanoi, Viet Nam*
[3] *Advanced Institute for Science and Technology, Hanoi University of Science and Technology, No.1 Dai Co Viet Street, 100000 Hanoi, Viet Nam*

***Corresponding author e-mails:** tu.nguyencong@hust.edu.vn, lam.nguyenhuu@hust.edu.vn*

Abstract

WO_3 nanoplate synthesized by acid precipitation method was composited with commercial carbon nanotube with different weight percents (0.5, 1.0, and 1.5 wt% of CNT). The ammonia gas sensing characteristics of composite materials at low temperature (50°C) were investigated and compared with that of pristine materials (WO_3 nanoplate, commercial carbon nanotube). The results showed that the composition enhanced the gas sensing properties in comparison with the pristine carbon nanotube-based sensor and more stable than pristine WO_3 nanoplate-based sensor. The response of gas sensors to 30 ppm of ammonia got the highest value of 45% in 0.5 wt%-CNT sensor – enhanced 100 times in comparison with carbon nanotube-based sensor. The calculated limit of detection of 0.5 wt%CNT/WO_3 sensor was at sub-trace-level of 3 ppb. This enhancement shows the high applicability of composite materials in gas sensor working at room temperature

1. Introduction

Ammonia (NH_3) is a hazardous, colorless gas and is widely used in industry, agriculture, and breeding. In the human breath, NH_3 concentration is in the range of 50-2000 ppb and could be used as an indicator of kidney, liver dysfunctions as well as stomach diseases [1]. Nowadays, most of the NH_3 gas sensor are conductometric sensors and are based on metal oxide semiconductors such as SnO_2, WO_3, ... which have high working temperatures (normally higher than 200°C) [2]. The high working temperature results in the complex design of the sensor device with the heating part embedded in the device. Moreover, metal oxide semiconductor-based NH_3 gas sensors usually have high resistance resulting in low readout-signal, and require the amplification part in the device which causes the sensor device to be more complex and consume more power [3]. Because of the above reasons, recently many efforts have been devoted to find the proper nanomaterials which have suitable resistance and low-working temperature (< 200°C) [4–7]. Carbon nanotube (CNT) appears to be one of the promising active materials for NH_3 gas sensor which could work at low temperatures or even at room temperature (RT) [8]. The drawback of CNT is the poor response with NH_3. To overcome this drawback, D. Zhang et. al. composited CNT with polyaniline and MoS_2 to use the high conductivity of CNT [4]; A. G. Bannov et. al. modified CNT surface by plasma treatment to increase the active point on the CNT surface [5]; N. Q. Lich et. al. functionalized CNT surface with Co nanoparticles to enhance the response [7]; P. Muthukumaran et. al. enhance the selectivity to NH_3 by mixing Fe_2O_3 nano-dendritic like-pine tree with CNT [9], X. Lina. et. al. composited functionalized CNT with polyaniline to enhance the response of CNT-based NH_3 gas sensor at RT [10].

To improve the response of CNT-based NH_3 gas sensor, in this paper, commercial CNT was composited with WO_3 nanoplates (NPs) synthesized by acid precipitation method with different CNT content (0.5, 1.0, and 1.5 wt%). The NH_3 gas sensivity of nanocomposite materials-based sensors was investigated at 50°C (low temperature) and compared with that of pristine-CNT-based, and pristine-WO_3-based sensors. The obtained results showed that nanocomposite-based sensors had better performance parameters in compare with CNT-based sensor, and more stable than WO_3 NP-based sensor. The detection limit and the selectivity of the best-performance nanocomposite-based sensor was also calculated.

2. Experiments

2.1 Synthesis WO_3 NPs and composite of CNT/WO_3 NPs

Dissolving 8.25 g sodium tungstate hydrate ($Na_2WO_4 \cdot 2H_2O$) into 25 ml distilled water. A yellow slurry solution was obtained after gradually dropping

45 ml chlorhydric acid (HCl, 37 wt%) into the above solution. Adding 10 ml distilled water and stirring steadily the obtained solution for 4 h, then pouring into 100-ml Teflon lined autoclave. The acid precipitation process was carried out by keeping the autoclave at room temperature for 48 h. The strong yellow precipitation obtained after acid precipitation progress was cleaned and filtered by distilled water and filter paper (15.0 micron). Drying the cleaned slurry at 80°C for 24 h. The dried powder was then ground by agate mortar and pestle. Annealing the ground powder at 300°C for 2h in ambient air to get the WO_3 powder used for further study.

Dispersing 0.1 g of annealed WO_3 powder into 5 ml Dimethyl Formamide (DMF) to get a solution of WO_3. A solution of CNT was obtained by dispersing 0.1 g commercial multi-walled CNT (Shenzhen Nanotech, diameter: 60-100 nm, length: 2 μm). Mixing two solutions of WO_3 and CNT with different volume ratio to get mixing solutions of CNT/WO_3 with different CNT contents (0.5, 1.0, and 1.5 wt%).

2.2 NH₃ gas sensor: fabrication and characterization

Using Micropipette (0.5-10 μl, Phoenix Germany Instrument) to drop 0.5 μl of CNT/WO_3 mixed solutions on SiO_2/Si substrate which had been patterned with Pt electrodes (fabricated by microelectronic technology). Then drying for 10 mins at 80 °C. Repeating the above process two more times. The obtained samples were then annealed at 200 °C for 2 h to burn out DMF. The CNT-based and WO_3 nanostructure-based sensor were also fabricated by the same progress.

The NH_3 gas sensitivity characteristic of sensors was characterized by the revolution of sensor resistance when exposing to analytic gas – NH_3. Keithley 6487 was used to measure the resistance of sensors. The testing NH_3 concentration was determined by Canadian BW Gas Alert device. The humidity of the environment was stabilized at approximately ~50% during the measurement. The crystal properties of WO_3 powders were analyzed by X'pert Pro MPD using Cu-Kα source (λ=1.54056 Å), scanning rate 0.03°/2s, with the angle range of 20-70°.

The field effect scanning electron microscope (FESEM) JEOL JSM-7600F was utilized for morphology

analysis. Micro Raman spectra of samples observed by Renishaw Invia Raman Microscope using 633-nm laser, 12.5-mW excitation power was used to qualitatively analyze the component of composite materials.

3. Results and discussion

3.1 Structure and morphology of WO₃ nanoplates

Figure 1(a) was FESEM image of as-grown WO_3 sample. The as-grown WO_3 had uniform morphology of nanoplate with the mean dimensions of 150×150×40 nm. After annealing at 300°C, the obtained WO_3 also had uniform square nanoplate morphology of the size 150×150 nm but a smaller thickness of ~10 nm (Figure 1(b)). The annealed WO_3 nanoplates were well separated and had sharper corners. The change from thick nanoplate to thin nanoplate was explained by the delamination of the thick plate during the annealing process.

The annealing not only caused the change of morphology but also make the transition of crystal structure which was observed in X-Ray diffraction (XRD) analysis. Figure 1(c) manifested the XRD spectra of as-grown WO_3 powder and annealed WO_3 powder. The XRD analysis using HighScore Plus software with ICDD database showed that as-grown WO_3 powder was orthorhombic $WO_3.H_2O$ (card no ICDD 01-084-0886) having (111) dominant plane; the annealed WO_3 powder was WO_3 having the stable monoclinic phase (ICDD card no 01-083-0951)[11]. The changing from orthorhombic $WO_3.H_2O$ to monoclinic WO_3 was caused by the dehydration process happening during the calcination at 300°C for 2 h, which also caused the delamination of thick nanoplates $WO_3.H_2O$ into thin nanoplates WO_3 observed in FESEM analysis. The monoclinic WO_3 had three dominant planes: (002), (020), and (200) which had high surface energies in comparison with plane (111) [12]. The transfer from orthorhombic $WO_3.H_2O$ nanoplate to monoclinic WO_3 nanoplate through annealing at 300 °C is similar to the results reported by Ng et al. [13] and Sanasi et al. [14]. The thin square nanoplate morphology with dominant high surface-energy planes was very promising for NH_3 gas sensor application [12].
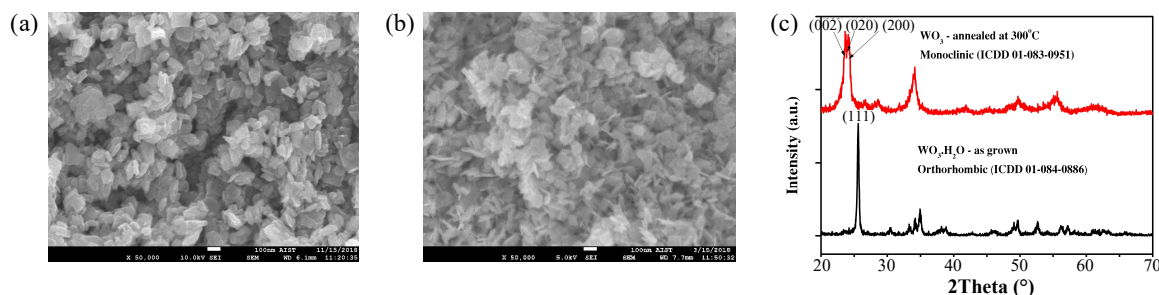

Figure 1. FESEM images of as-grown WO_3 nanostructures (a) and WO_3 nanostructures after annealing at 300°C for 2h (b). XRD spectra of as-grown WO_3 powder and annealed WO_3 powder (c).

The annealing not only caused the change of morphology but also make the transition of crystal structure which was observed in X-Ray diffraction (XRD) analysis. Figure 1.c manifested the XRD spectra of as-grown WO_3 powder and annealed WO_3 powder. The XRD analysis using HighScore Plus software with ICDD database showed that as-grown WO_3 powder was orthorhombic $WO_3.H_2O$ (card no ICDD 01-084-0886) having (111) dominant plane; the annealed WO_3 powder was WO_3 having the stable monoclinic phase (ICDD card no 01-083-0951)[11]. The changing from orthorhombic $WO_3.H_2O$ to monoclinic WO_3 was caused by the dehydration process happening during the calcination at 300°C for 2 h, which also caused the delamination of thick nanoplates $WO_3.H_2O$ into thin nanoplates WO_3 observed in FESEM analysis. The monoclinic WO_3 had three dominant planes: (002), (020), and (200) which had high surface energies in comparison with plane (111) [12]. The transfer from orthorhombic $WO_3.H_2O$ nanoplate to monoclinic WO_3 nanoplate through annealing at 300°C is similar to the results reported by Ng et al. [13] and Sanasi et al. [14]. The thin square nanoplate morphology with dominant high surface-energy planes was very promising for NH₃ gas sensor application [12].

3.2 Nanocomposites analyzing

Figure 2(a) was FESEM image of 0.5%CNT/WO_3 nanocomposite-based sensor. The image clearly showed that CNTs was well dispersed into the matrix of WO_3 NPs, and the mixing process did not affect the morphology of WO_3 NPs. The similar results were also observed in other nanocomposite-based sensors. The appearance of CNT in the nanocomposites was also confirmed through analyzing the Raman spectra of composite samples (Figure 2(b)). In the Raman spectra of composite samples, the co-appearance of the typical peaks of monoclinic WO_3 and multi-walled CNT were clearly shown. The typical peaks of monoclinic WO_3 were at 270.6, 711.9, and 804.8 cm^{-1} corresponding to the bending vibration - δ(O-W-O) - and stretching vibrations - ν(O-W-O) - of O-W-O binding in monoclinic WO_3 structure, respectively [13,14]. The bands at 1327.0 and 1571.5 cm^{-1} were typical D-band and G-band originating from the vibration of dis-ordered defects and graphite layer in CNT, respectively [17]. The ratio between the intensity of peaks of CNT and peaks of WO_3 increased with the increasing of CNT content in the nanocomposite. The Raman analysis confirmed the co-appearance of CNT and WO_3 in the nanocomposite. The position of typical peaks of WO_3 and CNT in nanocomposites were extracted and reported in Table 1.
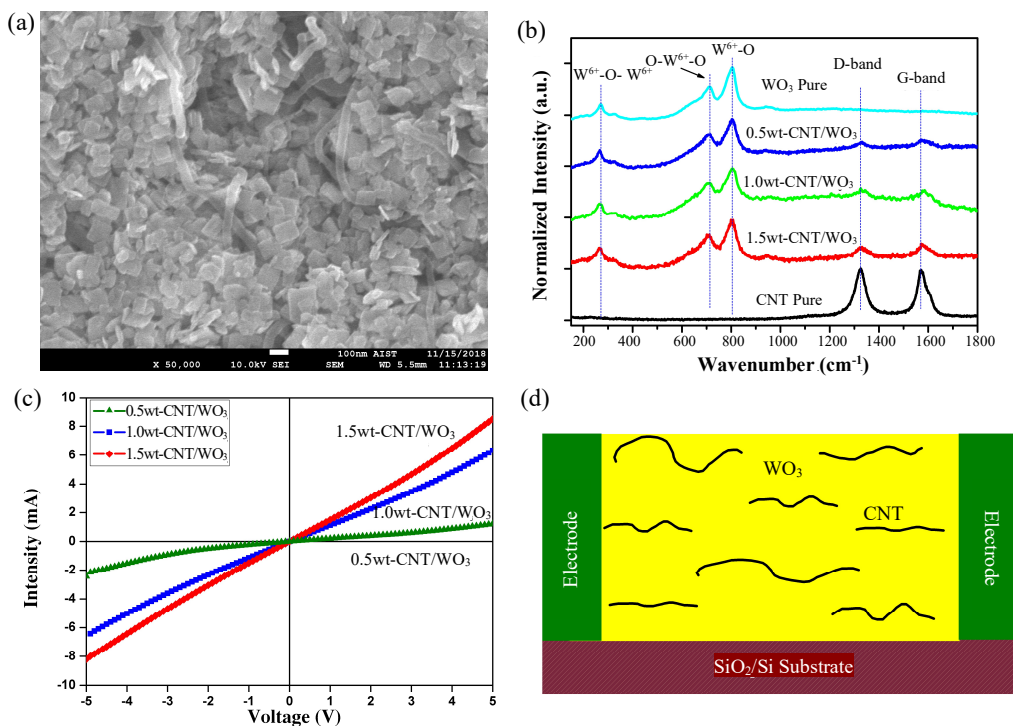

Figure 2. (a) FESEM image of the surface of 0.5%CNT/WO_3 nanocomposite-based sensor; (b) Micro Raman spectra of CNT-based, WO_3 nanoplate-based, and CNT/WO_3 nanocomposite-based sensors; (c) I-V curves of CNT/WO_3 nanocomposite-based sensors at 50°C; (d) The scheme of nanocomposite.

Table 1. The position (cm^{-1}) of typical peaks of WO$_3$ monoclinic and CNT in pristine and nanocomposite samples.

Raman vibration	100%CNT	1.5%CNT/WO$_3$	1.0%CNT/WO$_3$	0.5%CNT/WO$_3$	WO$_3$
δ(O-W-O)	-	265.7	266.4	267.1	270.6
ν(O-W-O)	-	707.7	708.3	710.2	711.9
	-	803.0	803.5	804.2	804.8
G-band	1571.5	1574.9	1575.6	1574.1	-

From data in Table 1, the shifts of typical peaks of both WO$_3$ and CNT were clearly observed. The G-band signal of CNT was up-shifted from 1571.5 cm^{-1} in pristine CNT to 1574.9, 1575.6 and 1574.1 cm^{-1} in nanocomposite with 1.5, 1.0 and 0.5 % CNT, respectively. The peaks of stretching vibrations ν(O-W-O) of WO$_3$ were down-shifted to lower wavenumber: peak at 804.8 in pure WO$_3$ was transfered to 804.2, 803.5 and 803.0 cm^{-1}; peak at 711.9 cm^{-1} in pure WO$_3$ was moved to 710.2, 708.3 and 707.7 cm^{-1} in 0.5, 1.0 and 1.5%CNT nanocomposites, respectively. The peak of bending vibration of WO$_3$ δ(O-W-O) was also shifted from 270.6 to 267.1, 266.4 and 265.7 cm^{-1} when CNT content increased from 0 to 0.5, 1.0 and 1.5% in nanocomposite. These shifts confirmed that there was interaction – charge transfer - between CNT and WO$_3$ NP in the CNT/WO$_3$ NP nanocomposite [18].

One of the criteria for gas sensing nanocomposite material was having the proper conductivity, which could, in consequence, reduce the resistance of the sensor to the range of tens kΩ to employ in low-power consumption and high signal-readout sensor [3]. In Figure 2(c), there are the I-V curves of nanocomposite-based sensors at 50°C. All I-V curves of nano-composite-based sensors showed the characteristic of Ohmic contact. The resistances of nanocomposite sensors were in the range of hundreds of Ohms to several kilo-Ohms. When the CNT content in the sample increased from 0 to 0.1, 0.3 and 0.5%, the resistance decreased from 1040 to 15.1, 1.0 and 0.64 kΩ, respectively. This decreasing was due to the dispersing of CNT in WO$_3$ NPs matrix as shown in Figure 2(d). These results showed that CNT/WO$_3$ NPs nanocomposite materials were suitable for active material in low-power consumption gas sensor. Moreover, from the revolution of resistance of nanocomposite-based sensor with CNT content, we could infer that in the nanocomposite CNT acted as conductive part and kept the vital role in the modulating the resistance of the nanocomposite-based sensors.

3.3 Ammonia gas sensing properties

The gas sensitivity of the sensor was characterized by the response, response time and recovery time. The response was determined by the ratio (R$_{gas}$-R$_{air}$)/ R$_{air}$ where R$_{air}$ and R$_{gas}$ were resistances of the sensor in dry air and when exposing to the analyte gas – NH$_3$, respectively. Response time and recovery time were the time it takes to take 90% of the change of resistance in the response and recovery process, respectively. The time evolution of responses of all investigated sensors with 30 ppm NH$_3$ at 50°C were presented in Figure 3(a)-3(e). All sensors showed the p-type response in which resistance increased when exposing to reducing gas NH$_3$. The response of pristine-CNT-based sensor was 0.45%. The responses of 0.5%CNT/WO$_3$, 1.0%CNT/WO$_3$, 1.5%CNT/WO$_3$ nanocomposite-based sensors were 46, 0.8, and 1.4%, respectively. The WO$_3$ NPs-based sensor responded well with NH$_3$ but not steadily as CNT-, or nanocomposite-based sensors (Figure 4(e)). In comparison with the CNT-based sensor, all nanocomposite-based sensor had higher responses, especially 0.5%CNT/WO$_3$ nanocomposite-based sensor having 100-time higher response than that of CNT-based sensor (Figure 4(f)). The response time and recovery time of 0.5%CNT/WO$_3$ sensor were also shorter in comparison with these time of CNT-based sensor. The response, response time and recovery time of sensors were all showed in Table 2.

In the nanocomposite-based sensors, the sensor made of 0.5%CNT/WO$_3$ nanocomposite showed the highest performance with the highest response, shorter response and recovery times than CNT-based sensor (Table 2). When CNT content increased to 1.0%, the response was 2-times higher and response time was 2-times shorter than CNT-based sensor, but had longer recovery time. Continuing increased CNT content to 1.5%, the response increased to 3-time higher, but both response and recovery time are longer than CNT-based sensor. These difference enhancements were due to the content of CNT which resulted in the different time for analyte gas dispersing into the sensor.

We continued to investigate NH$_3$ gas sensitivity at RT of the 0.5%CNT/WO$_3$ nanocomposite-based sensor which showed the highest performance parameters. Figure 4.a was the revolution of response with different testing gas NH$_3$ concentration in the range from 30 to 70 ppm. The results showed that, at RT, the response of 0.5%CNT/WO$_3$ was remarkably higher than working at 50°C (125% in comparison with 45%). These results implied that 0.5%CNT/WO$_3$ with simply synthesis method could be a promising material for NH$_3$ gas sensor at RT.
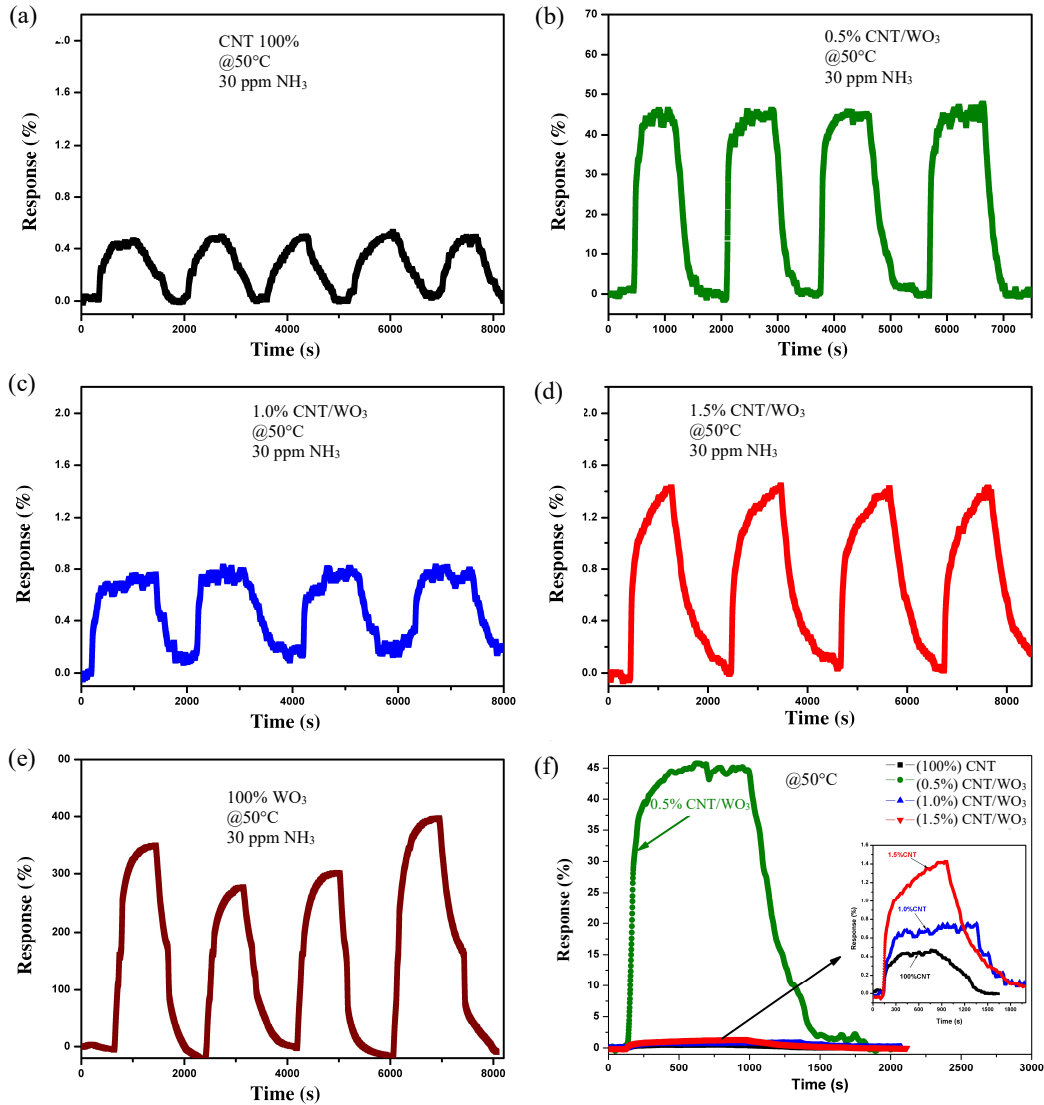
Figure 3. The time evolution of response of sensors with 30 ppm NH₃ at 50°C: (a) CNT-based sensor, (b) 0.5%CNT/WO₃, (c) 1.0%CNT/WO₃, (d) 1.5%CNT/WO₃ nanocomposite-based sensor, and (e) WO₃ NP-based sensor. (f) The comparison of the response of CNT-based and nanocomposite-based sensors.
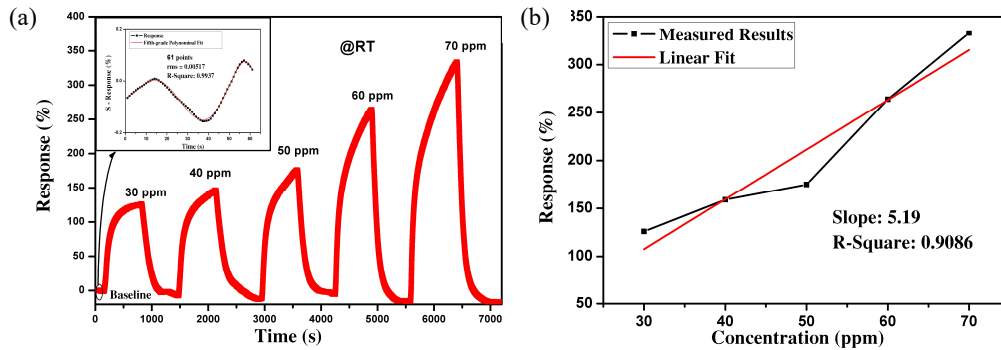

Figure 4. (a) The revolution of the response of the 0.5wt% CNT/WO₃ NP nanocomposite-based sensor with different concentration of NH₃ gas. The inset picture is the fifth-grade polynomial fitting of the baseline of the response line; (b) The linear fitting of response versus NH₃ concentration of 0.5wt% CNT/WO₃ NP nanocomposite-based sensor.
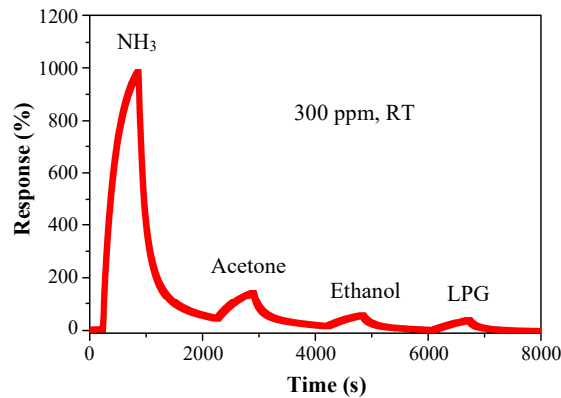
Figure 5. The response of 0.5wt% CNT/WO₃ NP nanocomposite-based sensor with 300 ppm of different testing gas at room temperature: NH₃, acetone, ethanol and LPG.

From the revolution of response with different concentration of testing gas at RT, we calculated the theoretical detection limit (DL) of 0.5%CNT/WO₃ nanocomposite-based sensor at RT. The DL was determined based on the condition of the ratio of signal to noise, in which DL was calculated using the following formula:

$$DL(ppm) = 3 \times \frac{rms}{slope} \qquad (1)$$

where *rms* was determined through fitting the baseline of response with fifth-grade polynomial (inset of Fig. 4°); slope was determined from linear fitting the response of sensor with different concentration of testing gas (Figure 4(b)) [3]. Our calculation showed that, at RT, 0.5%CNT/WO₃ nanocomposite-based sensor had $rms = 0.00517$, $slope = 5.19$, and $DL = 0.003$ ppm = 3 ppb. With the detection limit of 3 ppb, the 0.5%CNT/WO₃ nanocomposite showed a promising applicability in detecting trace-level of NH₃ gas such as in human breath to early diagnose the disease of kidney, liver [1].

Table 2. The response time, recovery time, and response of CNT-based and nanocomposite-based sensors with 30 ppm of NH₃ at 50°C.

Samples	Response time (s)	Recovery time (s)	Response (%)
100% CNT	200	515	0.45
0.5%CNT/WO₃	170	350	46
1.0%CNT/WO₃	100	600	0.8

The selectivity of sample 0.5% CNT/WO₃ NP with NH₃ in comparison with acetone, ethanol and LPG (Liquefied Petrolium Gas) at Rt was also studied. Figure 5 manifested the response of nanocomposite sample 0.5% CNT/WO₃ NP with different gas (NH₃, acetone, ethanol and LPG) with the same concentration of 300 ppm. The response of sensor with 300 ppm testing gas of NH₃, acetone, ethanol and LPG were 983,

142, 55 and 38 %, respectively. These results showed that 0.5% CNT/WO₃ sensor was more selective to NH₃ than other testing gas (acetone, ethanol and LPG). This selectivity to NH₃ of 0.5% CNT/WO₃ NP sample was similar to the selectivity of Co-decorated CNT reported by Lich *et al.* [7].

3.4 Gas sensing mechanism of nanocomposite materials

The enhancement of ammonia gas sensing of nanocomposite materials might be explained as following: WO₃ was a natural n-type sensing material, but at low temperature, the inversion layer appeared on the surface of WO₃ nanostructures which change the behavior of WO₃ from n-type to p-type [16,17]. The inversion layer strongly depended on oxygen and water concentration in the environment, this was the reason for the instability of WO₃ based sensor at low temperature [16,18]. In composition with CNT, the inversion effect was stabilized through same type contact - p-p contact - in which CNT acted as hole tank to conciliate the hole from the inversion layer on surface WO₃ nanostructure [2,16]. The reinforcement of carrier – charge transfer - from the WO₃ inversion layer was the reason for the enhancement of nanocomposite-based sensor in comparison with CNT-, and WO₃ - based sensor. The charge transfer beween WO₃ and CNT was confirmed by the shifts of typical Raman peaks of WO₃ and CNT in nanocomposites mentioned above. Moreover, due to the typical morphology of WO₃ NPs – large thin plate with dominant active planes – (002), (020), and (200) - the responses of nanocomposite-based sensors were improved in comparison with pristine CNT-based sensor [12].

4. Conclusions

In summary, we have synthesized nanocomposite materials of WO₃ nanoplates and commercial multi-walled CNTs with different weight contents of CNT (0.5, 1.0, and 1.5 wt%) by a simple mixing process.

Nanocomposite-based sensors responded well to NH_3 gas at low temperature (50ºC). The responses of nanocomposite-based sensors were higher than the pristine-CNT-based sensor and were more stable than pristine-WO₃ NP-based sensor. 0.5wt%-CNT nano-composite-based sensor showed the highest response of 45% which was 100-times higher than the pristine-CNT-based sensor. At RT, 0.5wt%-CNT-based sensor showed higher exploitation parameters: the response reached to a higher value of 125%, the theoretical detection limit was 3 ppb, the selectivity to NH_3 gas in comparison with acetone, ethanol and LPG. This enhancement of the NH_3 sensitivity was assigned to the synergistic effect in nanocomposite materials. The mechanism of the synergistic effect is still needed more research to make clear. Our results showed that CNT/WO₃ NP-based nanocomposite had prosperous potential in NH_3 gas sensor working at room temperature.

5. Acknowledgments

References

[1] S. Abdulla, D. V. Ponnuvelu, and B. Pullithadathil, "Rapid, trace-level ammonia gas sensor based on surface-engineered Ag nanoclusters@poly-aniline/multiwalled carbon nanotubes and insights into their mechanistic pathways," *Chemistry Select*, vol. 2, pp. 4277-4289, 2017.

[2] P. T. Moseley, "Progress in the development of semiconducting metal oxide gas sensors: A review," *Measurement Science and Technology*, vol. 28, p. 82001, 2017.

[3] J. Li, Y. Lu, Q. L. Ye, J. Han, and M. Meyyappan, "Carbon nanotube based chemical sensors for gas and vapor detection," *Nano Letters*, vol. 3, pp. 929-933, 2003.

[4] D. Zhang, Z. Wu, P. Li, X. Zong, G. Dong, and Y. Zhang, "Facile fabrication of polyaniline/ multi-walled carbon nanotubes/molybdenum disulfide ternary nanocomposite and its high-performance ammonia-sensing at room temperature," *Sensors and Actuators B: Chemical*, vol. 258, pp. 895-905, 2018.

[5] A. G. Bannov, O. Jasek, A. Manakhov, M. Marik, D. Necas, and L. Zajickova, "High-performance ammonia gas sensors based on plasma treated carbon nanostructures," *IEEE Sensors Journal*, vol. 17, no. 7, pp. 1964-1970, 2017.

[6] J. Zhang, X. Liu, G. Neri, and N. Pinna, "Nanostructured materials for room-temperature gas sensors," *Advanced Materials*,

[7] L. Q. Nguyen, P. Q. Phan, H. N. Duong, C. D. Nguyen, and L. H. Nguyen, "Enhancement of NH_3 gas sensitivity at room temperature by carbon nanotube-based sensor coated with Co nanoparticles," *Sensors*, vol. 13, pp. 1754-1762, 2013.

[8] M. M. Rana, D. S. Ibrahim, M. R. Mohd Asyraf, S. Jarin, and A. Tomal, "A review on recent advances of CNTs as gas sensors," *Sensor Review*, vol. 37, pp. 127-136, 2017.

[9] P. Muthukumaran, C. Sumathi, J. Wilson, C. Sekar, S. G. Leonardi, and G. Neri, "Fe₂O₃/ Carbon nanotube-based resistive sensors for the selective ammonia gas sensing," *Sensor Letters*, vol. 12, pp. 17-23, 2014.

[10] L. Xue, W. Wang, Y. Guo, G. Liu, and P. Wan, "Flexible polyaniline/carbon nanotube nano-composite film-based electronic gas sensors," *Sensors and Actuators B: Chemical*, vol. 244, pp. 47-53, 2017.

[11] Z. F. Huang, J. Song, L. Pan, X. Zhang, L. Wang, and J. J. Zou, "Tungsten oxides for photocatalysis, electrochemistry, and photo-therapy," *Advanced Materials*, vol. 27, pp. 5309-5327, 2015.

[12] M. D'Arienzo, L. Armelao, C. M. Mari, S. Polizzi, R. Fuffo, R. Scotti, and F. Morazzoni, "Surface interaction of WO₃ nanocrystals with NH_3. Role of the exposed crystal surfaces and porous structure in enhancing the electrical response," *RSC Advances*, vol. 4, pp. 11012-11022, 2014.

[13] C. Y. Ng, K. Abdul Razak, and Z. Lockman, "Effect of annealing on acid-treated WO₃·H₂O nanoplates and their electrochromic properties," *Electrochimica Acta*, vol. 178, pp. 673-681, 2015.

[14] T. Sanasi, S. Pinitsoontorn, M. Horprathum, P. Eiamchai, C. Chananonnawathorn, and W. Hinchreeranun, "Development of WO₃ nano-structure by acid treatment and annealing," *Journal of Metals Materials and Minerals*, vol. 27, pp. 6-11, 2017.

[15] M. F. Daniel, B. Desbat, J. C. Lassegues, B. Gerand, and M. Figlarz, "Infrared and Raman study of WO₃ tungsten trioxides and WO₃.xH₂O tungsten trioxide hydrates," *Journal of Solid State Chemistry*, vol. 67, pp. 235-247, 1987.

[16] C. V Ramana, S. Utsunomiya, R. C. Ewing, C. M. Julien, and U. Becker, "Structural stability and phase transitions in WO₃ thin films," *Journal of Physical Chemistry B*, vol. 110, pp. 10430-10435, 2006.

[17] M. S. Dresselhaus, A. Jorio, and R. Saito, "Characterizing graphene, graphite, and carbon nanotubes by Raman spectroscopy," *Annual Review of Condensed Matter Physics*, vol. 1, no. 1, pp. 89-108, 2010.

[18]   L. Bokobza and J. Zhang, "Raman spectroscopic characterization of multiwall carbon nanotubes and of composites," *Express Polymer Letters*, vol. 6, pp. 601-608, 2012.

[19]   Y. Wei, M. Hu, D. Wang, W. Zhang, and Y. Qin, "Room temperature NO_2- sensing properties of porous silicon/tungsten oxide nanorods composite," *Journal of Alloys and Compounds*, vol. 640, pp. 517-524, 2015.

[20]   D. Nguyen Dac, V. Dang Duc, and C. Nguyen Duc, "Hydrothermal synthesis and NH_3 gas sensing property of WO_3 nanorods at low temperature," *Advances in Natural Sciences: Nanoscience and Nanotechnology*, vol. 6, pp. 035006-035011, 2015.

[21]   W. Yan, M. Hu, P. Zeng, S. Ma, and M. Li, "Room temperature NO_2-sensing properties of WO_3 nanoparticles/porous silicon," *Applied Surface Science*, vol. 292, pp. 551-555, 2014.